MNRAS Advance Access published November 3, 2016

Non-monotonic spatial distribution of the interstellar dust in astrospheres: finite gyroradius effect

O. A. Katushkina[1⋆], D. B. Alexashov[1,2], V. V. Izmodenov[1,2,3] and V. V. Gvaramadze[1,4,5]

[1] *Space Research Institute of Russian Academy of Sciences, Profsoyuznaya Str. 84/32, Moscow, 117335, Russia*
[2] *Institute for Problems in Mechanics, prosp. Vernadskogo 101, block 1, Moscow, 119526, Russia*
[3] *Lomonosov Moscow State University, GSP-1, Leninskie Gory, Moscow, 119991, Russia*
[4] *Sternberg Astronomical Institute, Moscow State University, Universitetskij Pr. 13, Moscow 119992, Russia*
[5] *Isaac Newton Institute of Chile, Moscow Branch, Universitetskij Pr. 13, Moscow 119992, Russia*

Accepted yyyy month dd. Received yyyy month dd; in original form yyyy month dd

ABSTRACT

High-resolution mid-infrared observations of astrospheres show that many of them have filamentary (cirrus-like) structure. Using numerical models of dust dynamics in astrospheres, we suggest that their filamentary structure might be related to specific spatial distribution of the interstellar dust around the stars, caused by a gyrorotation of charged dust grains in the interstellar magnetic filed. Our numerical model describes the dust dynamics in astrospheres under an influence of the Lorentz force and assumption of a constant dust charge. Calculations are performed for the dust grains with different sizes separately. It is shown that non-monotonic spatial dust distribution (viewed as filaments) appears for dust grains with the period of gyromotion comparable with the characteristic time scale of the dust motion in the astrosphere. Numerical modelling demonstrates that number of filaments depends on charge-to-mass ratio of dust.

Key words: shock waves – methods: numerical – circumstellar matter – dust, extinction.

1 INTRODUCTION

Astrospheres are the structures formed around stars because of interaction between the stellar wind (SW) and the surrounding interstellar medium (ISM). One well-known example of an astrosphere is the heliosphere around the Sun. The shape of a particular astrosphere is determined by the properties of the SW and the local ISM. Differences in these properties may lead to a wide range of shapes of observed astrospheres (Sahai & Chronopoulos 2010; Gvaramadze et al. 2011a; Peri et al. 2012; Decin et al. 2012; Cox et al. 2012; Peri, Benaglia & Isequilla 2015; Kobulnicky et al. 2016).

The region of interaction between the supersonic SW and the supersonic ISM flow contains three discontinuities (see Fig. 1): (1) the stellar wind termination shock (TS), separating the region of freely flowing wind from the shocked wind, (2) the tangential discontinuity or the astropause (AP), which separates the material of the SW from that of the ISM, and at which the SW ram pressure is balanced by the ram pressure of the ISM, and (3) the forward shock or the bow shock (BS), separating the shocked ISM from the unperturbed one. For the first time, such a two-shock structure was considered for the heliosphere by Baranov, Krasnobaev & Kulikovskii (1971), who numerically obtained the shape of the AP under the thin-layer approximation. Later on, Wilkin (1996) applied this theory for the shape of the stellar wind BSs using the same approximation.

The thin-layer solution provides a good description of the shape of the BSs with efficient cooling, for which the thickness of the interaction region between the stellar wind and the ISM is much smaller than the characteristic scale of the BS. In this case the distance from the star to the BS at nose part of astrosphere is almost equal to the stand-off distance, R_0 that is the distance from the star to the AP in the upwind direction (Fig. 1). For a wind-blowing star moving with velocity $\mathbf{v}_*$ relative to the ISM of mass density $\rho_{\rm ISM}$, the stand-off distance is given by

$$R_0 = \sqrt{\frac{\dot{M} v_{\rm w}}{4\pi \rho_{\rm ISM} v_*^2}}\,, \qquad (1)$$

where $\dot{M}$ and $v_{\rm w}$ are the stellar wind mass-loss rate and velocity, respectively.

⋆ E-mail: okat@iki.rssi.ru

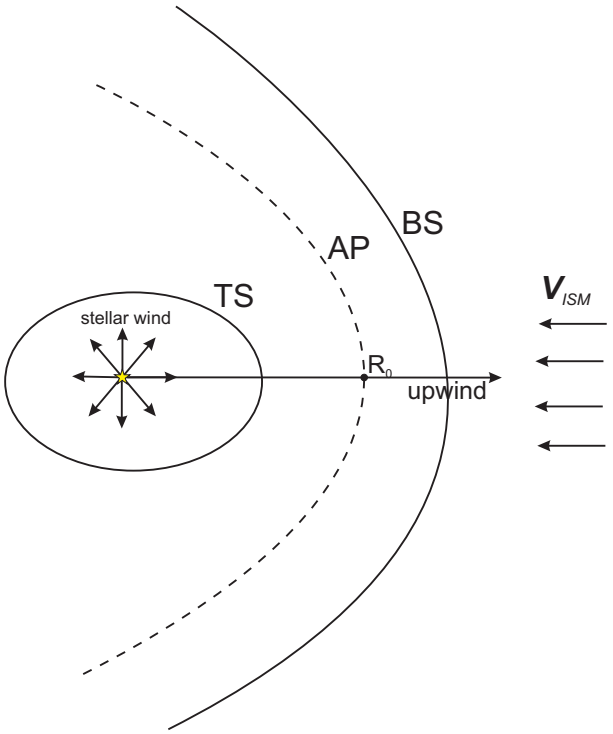

Figure 1. Schematic structure of an astrosphere. TS, AP and BS are, respectively, the termination shock, the astropause and the bow shock. The upwind is the direction of star's motion relative to the surrounded ISM. R_0 is the stand-off distance.

The assumption that the BS forms at the distance R_0 from the star is widely exploited in the astrophysical literature (e.g. to determine the properties of the stellar wind or the local ISM; Kobulnicky, Gilbert & Kiminki 2010; Gvaramadze, Langer & Mackey 2012; Peri et al. 2012) and the entire interaction region between the SW and the ISM is often called as the bow shock. In reality, however, the thickness of this region could be comparable with the characteristic scale of the astrosphere (e.g. van Buren 1993; Comerón & Kaper 1998). To avoid the terminological confusion, we call the two-shock structure as astrosphere and use the term "bow shock" in its classical gasdynamic and magnetohydrodynamic (MHD) meaning.

The astrospheres can be observed at various wavelengths, of which the mid-infrared waveband is most appropriate for their detection (van Buren et al. 1995; Gvaramadze & Bomans 2008; Peri et al. 2012). Numerical modelling of astrospheres around OB stars show that their infrared emission is mostly due to re-radiation of the starlight by the circumstellar and interstellar dust grains accumulated in the astrospheres (Meyer et al. 2014). Thus, to interpret the available images of astrospheres and to understand their gasdynamic or MHD structure one needs to analyze the dust distribution within them.

The high angular resolution of recent infrared surveys carried out with the *Spitzer Space Telescope*, *Wide-field Infrared Survey Explorer* (*WISE*) and *Herschel Space Observatory* allowed to resolve the fine structure of numerous astrospheres and showed that many of them have filamentary (cirrus-like) structure (France, McCandliss & Lupu 2007; Gvaramadze et al. 2011a,b; Peri et al. 2012; Decin et al. 2012; see also Fig. 2). The origin of this structure is not well understood. One can speculate that it is due to interstellar dust grains aligned with the local interstellar magnetic field, which re-radiate the light of central stars of the astrospheres (Gvaramadze et al. 2011b) or due to time dependent variations of the stellar wind parameters (Decin et al. 2012), or that it is caused by some kind of instabilities in the astrospheres (Dgani, Van Buren & Noriega-Crespo 1996).

In this paper, we present a new possible physical mechanism for formation of the cirrus-like structure of some astrospheres. Our results based on the three dimensional (3D) modelling of interstellar dust distribution in astrospheres produced by stars moving through the ISM with a large-scale homogeneous magnetic field. We show that the dust distribution strongly depends on the charge-to-mass ratio of dust grains as well as on the orientation of the magnetic field with respect to the direction of stellar motion. We also show that synthetic dust column density maps have filamentary structure if the dust gyroperiod is comparable with the characteristic time scale of the dust motion in the astrosphere. This could be an explanation of the observational data.

The paper is organized as follows. In Section 2, we describe our numerical 3D stationary MHD model of an astrosphere and the dust distribution within and around it. Results of the 3D simulations are presented in Section 3. Section 4 discusses limitations of our model. Summary and conclusions are presented in Section 5.

2 MATHEMATICAL FORMULATION OF THE PROBLEM

2.1 Numerical model for the plasma distribution in the astrosphere

At first, we present a 3D MHD model of the astrosphere around a wind-blowing star moving with velocity $\mathbf{v}_*$ through the uniformly magnetized ISM. Both the stellar wind and the ISM are assumed to be fully ionized. For the sake of simplicity, we restrict ourselves to the framework of ideal MHD and will not consider radiative cooling and thermal conduction, although these processes might be important for some astrospheres (see, e.g., Falle 1975; Weaver et al. 1977; Meyer et al. 2014). The governing equations are the steady-state ideal MHD equations:

$$\begin{aligned}
&\nabla\cdot(\rho\mathbf{v}_p)=0,\\
&\nabla\cdot\left[\rho\mathbf{v}_p\mathbf{v}_p+\left(p+\frac{B^2}{8\pi}\right)\mathsf{I}-\frac{\mathbf{BB}}{4\pi}\right]=0,\\
&\nabla\cdot\left[\left(\epsilon+p+\frac{B^2}{8\pi}\right)\mathbf{v}_p-\frac{(\mathbf{v}_p\cdot\mathbf{B})}{4\pi}\mathbf{B}\right]=0,\\
&\nabla\cdot[\mathbf{v}_p\mathbf{B}-\mathbf{B}\mathbf{v}_p]=0,\\
&\nabla\cdot\mathbf{B}=0,
\end{aligned}\tag{2}$$

where the variables have their usual meanings as ρ (plasma mass density), $\mathbf{v}_p$ (plasma velocity), p (thermal pressure), $\mathbf{B}$ (magnetic field), $\epsilon=\rho v^2/2+p/(\gamma-1)$ (kinetic plus internal energy per unit volume), γ (adiabatic index), and I is the unity tensor.

The inner boundary conditions for the uniform, spherically symmetric stellar wind taken at a sphere of radius r_s (inside TS) are the following: the stellar wind velocity is $v_{\rm w}$,

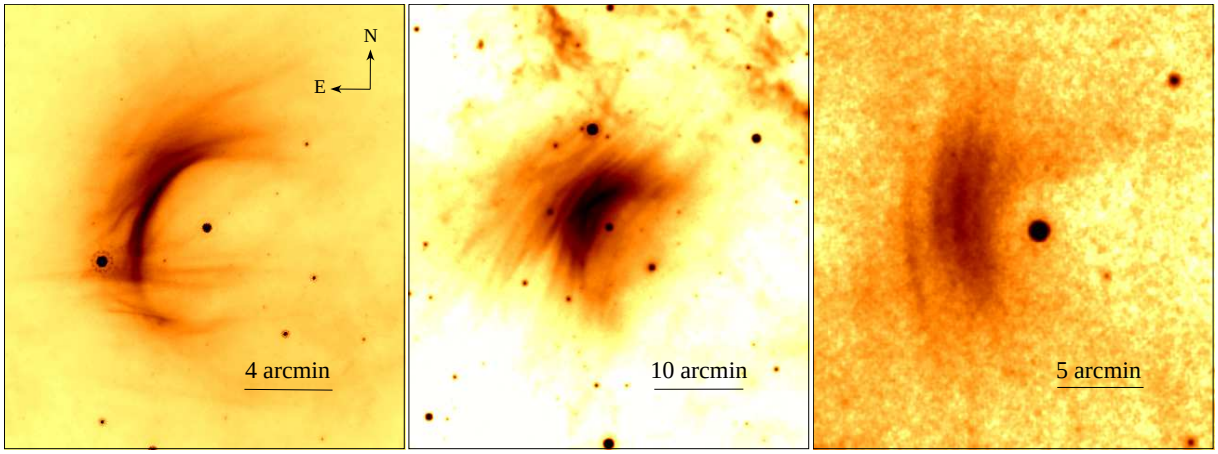

Figure 2. *Spitzer* 24 μm (left-hand panel) and *WISE* 22 μm (middle and right-hand panels) images of astrospheres associated with three early B stars, respectively, κ Cas, θ Car and β CMa. The orientation of the images is the same.

the density is $\rho_{\rm w} = \dot{M}/(4\pi v_{\rm w} r_s^2)$, and the thermal pressure is $p_{\rm w}$. The stellar wind is assumed to be non-magnetized. The unperturbed ISM is assumed to be uniformly magnetized with constant density ($\rho_{\rm ISM} = m_{\rm p} n_{\rm ISM}$, where $m_{\rm p}$ is a mass of proton, $n_{\rm ISM}$ is ISM number density), pressure ($p_{\rm ISM}$) or temperature ($T_{\rm ISM}$), and magnetic field ($\mathbf{B}_{\rm ISM}$). In the frame of reference of the star the ISM flows towards the star with velocity of $\mathbf{V}_{\rm ISM} = -\mathbf{v}_*$.

It can be shown that dimensionless solution of the formulated problem depends only on the sonic Mach number in the stellar wind, $M_{\rm w} = v_{\rm w}/\sqrt{\gamma p_{\rm w}/\rho_{\rm w}}$, the sonic and Alfvenic Mach numbers in the ISM, respectively, $M_{\rm ISM} = V_{\rm ISM}/\sqrt{\gamma p_{\rm ISM}/\rho_{\rm ISM}}$ and $M_{\rm A,ISM} = V_{\rm ISM}\sqrt{4\pi\rho_{\rm ISM}}/B_{\rm ISM}$, and the angle, α, between $\mathbf{V}_{\rm ISM}$ and $\mathbf{B}_{\rm ISM}$. In this work, we consider only hypersonic ($M_{\rm w} \gg 1$) winds, for which the structure of their astrospheres does not depend on the exact value of $M_{\rm w}$.

More details of the numerical method used to model the stellar wind-ISM interaction region can be found in Izmodenov and Alexashov (2015).

2.2 Model of the dust distribution in astrospheres

To calculate the dust distribution in the astrosphere we use a kinetic model developed previously for dust in the heliosphere and described in detail by Alexashov et al. (2016). In this work we consider the interstellar dust outside the astropause, where the filaments can be formed. A brief description of the model is following.

The dynamics of the interstellar charged dust grains outside of the astropause is determined by the Lorentz force $\mathbf{F}_{\rm L} = q[(\mathbf{v}_d - \mathbf{v}_p) \times \mathbf{B}]$, where q is the charge of a dust grain, $\mathbf{v}_d$ is the local velocity of dust, and $\mathbf{v}_p$ is the local velocity of plasma. Since we assume that the stellar wind is non-magnetized, $F_{\rm L} = 0$ inside the astropause. For massive hot stars the forces of gravitational attraction and radiation repulsion could be important even far away from the star. For example, Ochsendorf et al. (2014) have shown that the stellar radiation pressure of weak-wind B stars can sweep away the interstellar dust and force it to flow around the moving stars. In this study, to avoid mixing of different physical effects, we consider only the electromagnetic forces and neglect the radiation pressure and gravitation force.

Thus, trajectory of a dust grain is described by the following equation (in CGS units):

$$\frac{d\mathbf{v}_d}{dt} = \frac{q}{m \cdot c_0}[(\mathbf{v}_d - \mathbf{v}_p) \times \mathbf{B}], \qquad (3)$$

were, m is the mass of a dust grain, c_0 is the speed of light, $\mathbf{v}_d = \dot{\mathbf{x}}_d$, $\mathbf{x}_d$ is the position of a dust grain, and the plasma parameters $\mathbf{v}_p$ and $\mathbf{B}$ are taken from the MHD model of the astrosphere described in Section 2.1.

Initial conditions for equation (3) are defined in the unperturbed ISM, where we assume $\mathbf{v}_d = \mathbf{v}_p = \mathbf{V}_{ISM}$ (i.e. dust moves together with plasma), and, therefore, the Lorentz force is equal to zero.

In dimensionless form the equation of motion (3) becomes:

$$\dot{\hat{\mathbf{v}}}_d = a_d[(\hat{\mathbf{v}}_d - \hat{\mathbf{v}}_p) \times \hat{\mathbf{B}}], \qquad (4)$$

where the hatted variables are nondimensional and where there is only one parameter:

$$a_d = \frac{q}{m} \cdot \frac{R_0 \cdot \sqrt{\rho_{ISM}}}{c_0}. \qquad (5)$$

This is the dimensionless charge-to-mass dust ratio. Here, the charge q is expressed in CGS-units ($[q] = g^{1/2}\, cm^{3/2}\, s^{-1}$), R_0 is character distance of the astrosphere that is the stand-off distance defined in the Introduction.

We do not consider processes of dust charging and destruction, i.e. the charge and the mass of the dust grains are assumed to be constant. Correspondingly, the parameter a_d is constant for each dust grain and does not change along the trajectory. Note that $a_d \sim r_d^{-2}$ (because $q \sim r_d$, and $m \sim r_d^3$), where r_d is the radius of a dust grain, i.e. a_d is larger for smaller grains and vice versa.

To calculate the dust distribution the following procedure is used. We split 3D space by computational cells (plasma parameters and magnetic field are known and assumed to be constant for each grid cell), run a set of dust grains trajectories and then calculate dust number density

Table 1. Parameters of the model calculations.

No.	α	$M_{\rm ISM}$	$M_{\rm A,ISM}$	γ
1	90°	1.5	1.77	5/3
2	0°	1.89	1.77	1.0001

(n_d) and averaged velocity ($\mathbf{V}_{d,av}$) in each cell by counting the individual particles and their velocities and averaging over the cell.

In the next Section we present the results of modelling of the dust number density obtained for different values of parameter a_d.

3 RESULTS

In this work, we consider the effect of interstellar magnetic field on the dust distribution in astrospheres for two limiting cases of maximum and minimum possible thickness of the layer between the astropause and the bow shock. In the first so called "perpendicular case" the maximum thickness of the layer is achieved for adiabatic ($\gamma = 5/3$) flows with $\mathbf{B}_{\rm ISM} \perp \mathbf{V}_{\rm ISM}$ and $M_{\rm ISM} < M_{\rm A,ISM}$. In the second – "parallel case" the thickness of the layer is minimum for isothermal ($\gamma \approx 1$) flows with $\mathbf{B}_{\rm ISM} \parallel \mathbf{V}_{ISM}$. For this orientation of the magnetic field, the layer remains relatively thin even for adiabatic flows (see, e.g., Baranov & Zaitsev, 1995). The last isothermal case can be considered as a limit of maximum conductivity, i.e. it mimics the effect of thermal condition. Table 1 summarizes the parameters of our two model calculations.

3.1 Plasma and magnetic field distribution

Fig. 3 presents the results of model calculations for the two considered cases. The rectangular system of coordinates is the following: the Z-axis is opposite to $\mathbf{V}_{\rm ISM}$ and the X-axis lies in the plane ($\mathbf{B}_{\rm ISM}, \mathbf{V}_{\rm ISM}$). In the parallel case with $\mathbf{B}_{\rm ISM} \parallel \mathbf{V}_{\rm ISM}$ the problem is axisymmetric. Detailed analysis of the plasma distribution in the astrospheres is beyond the scope of this paper and it will be performed elsewhere. Here we briefly summarize the main features of the flows.

Fig. 3 shows that both in the perpendicular and parallel cases the plasma density is maximum between the TS and the AP, and shows a secondary maximum at the AP from the interstellar side. In the parallel case, the bow shock is much closer to the star compared with the perpendicular one. This is because of the assumed specific magnetic field configuration and the nearly isothermal character of the flow in the parallel case. In the perpendicular case, the magnetic field has a maximum at the nose part of the astrosphere beyond the AP, while in the parallel case there is a local minimum of magnetic field intensity at the critical point. This is because in the parallel case $\mathbf{v}_p \sim \mathbf{B}$ everywhere and $v_p = 0$ at the critical point. Distributions of the plasma velocity and magnetic field are critically important for behavior of the dust grains with small gyroradii.

Table 2. Parameters of the dust grains.

$a_{\rm d}$	$r_{\rm gyr}$	$D_{\rm gyr}$
5.4	0.01	0.125
3.6	0.015	0.188
1.8	0.032	0.375
1.08	0.053	0.649
0.72	0.068	1.025
0.36	0.129	2.148
0.18	0.547	4.495
0.09	1.598	7.799

All parameters are dimensionless (r_{gyr} and D_{gyr} are normalized to R_0). Gyroradius r_{gyr} is calculated at $z \approx 1.6$ for the dust particle moving at infinity along Z axis. D_{gyr} is an averaged distance that a dust grain passes along Z axis during one gyrorotational period.

3.2 Spatial dust distribution: formation of the filamentary structures

3.2.1 Perpendicular case

At first, we calculate the dust distribution for the perpendicular case. For the sake of simplicity, we do not consider a realistic mass and size spectrum of dust grains in the ISM (see, e.g., Mathis et al. 1977). Instead, we consider dust grains with several different values of a_d (see Table 2; parameters r_{gyr} and D_{gyr} presented in this Table as well are discussed in this section below).

Let us start from consideration of motion of the positively charged dust grains under an influence of the electromagnetic force $\mathbf{F}_{\rm L} = q(\mathbf{v}_d \times \mathbf{B} + \mathbf{E})$, where $\mathbf{E} = -\mathbf{v}_p \times \mathbf{B}$. As mentioned before, outside of the BS the supersonic interstellar plasma is undisturbed, i.e. both plasma and dust move together with velocity $\mathbf{V}_{\rm ISM}$, so that $F_{\rm L} = 0$. This means that with approaching to the BS all dust grains move freely along straight lines. Plasma flow decelerates at the BS, hence $v_d \neq v_p$ after crossing the BS and the Lorentz force appears. The Lorentz force initiates a gyrorotation of the dust grains around magnetic field lines. Radius of the gyromotion (gyroradius or Larmor radius) is $r_{gyr} = m\, v_\perp / |q|\, B$, where $v_\perp$ is the dust velocity component perpendicular to the magnetic field vector. In dimensionless form $\hat{r}_{gyr} = \hat{v}_\perp / (a_d \hat{B})$, meaning that particles with the largest a_d have the smallest gyrordius and vice versa.

The motion of a dust particle can be represented as the gyromotion around the magnetic field line frozen into the plasma and the motion of the guiding centre. The guiding centre velocity $\mathbf{V}_{gc}$ can be represented as a sum of the plasma velocity $\mathbf{v}_p$ (which is the velocity of the $\mathbf{E} \times \mathbf{B}$ drift) and the drift velocity $\mathbf{V}^d$ caused by the spatial gradients of the magnetic and electric fields, i.e. $\mathbf{V}_{gc} = \mathbf{v}_p + \mathbf{V}^d$. Note that along the most part of the dust trajectory the second drift velocity is negligible compared with the first one for the most considered dust particles. That is, the velocity of the guiding centre is almost equal to the plasma velocity.

Fig. 4A shows a trajectory ($x(z)$ and $y(z)$) of a dust grain (with the largest a_d of 5.4) started at the point P_0 ($x = 0$, $y = 0$, $z = 5.5$). Hereafter, all presented quantities (x, y, z, n_d, v_p, v_d, etc) are dimensionless: all distances are normalized to R_0, all velocities are normalized to $V_{\rm ISM}$,

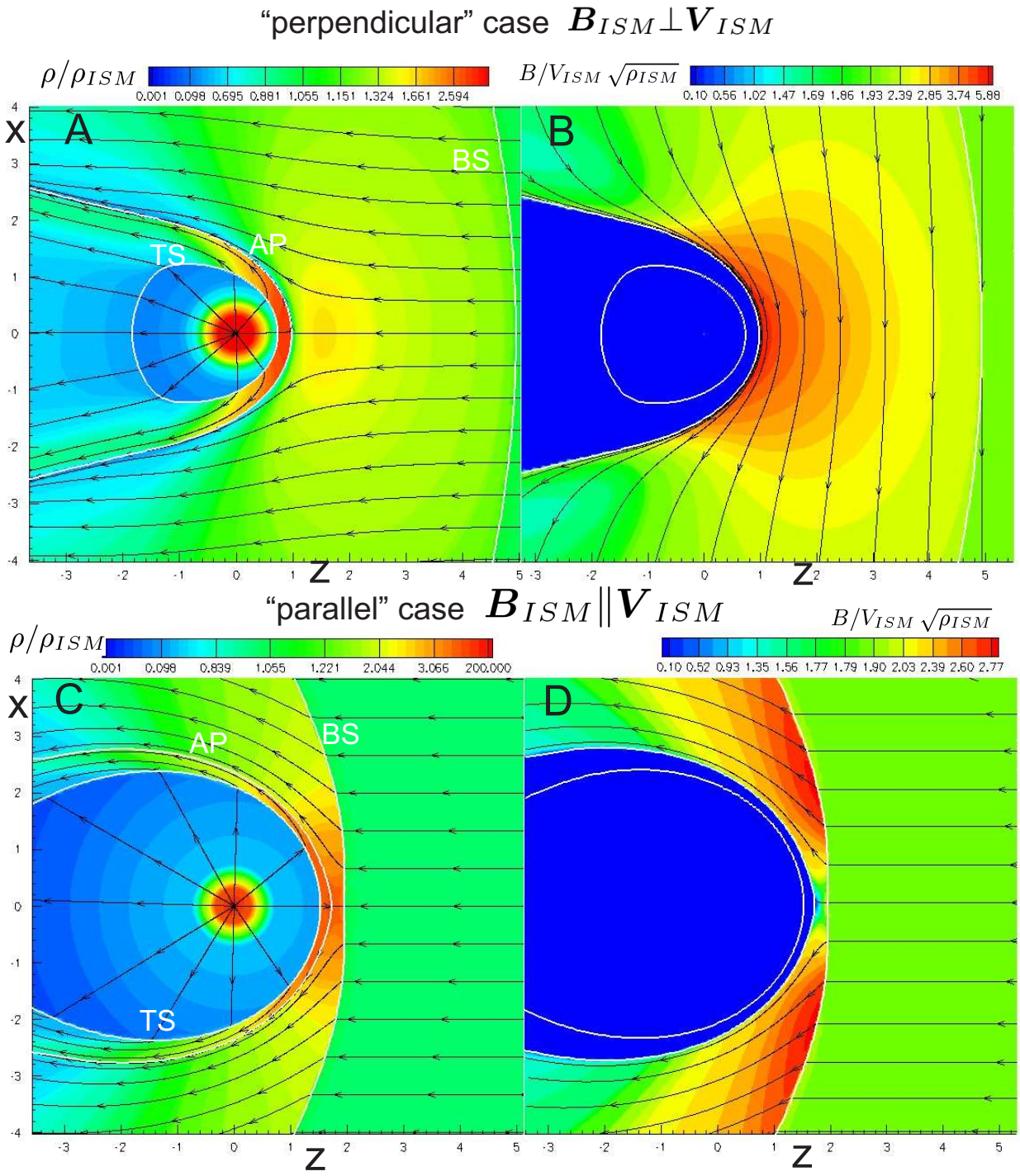

Figure 3. 2D distributions of the plasma density and streamlines (panels A and C) and the magnetic field with the magnetic field lines (panels B and D) in the (ZX)-plane for the perpendicular (panels A and B) and parallel (panels C and D) cases. The termination shock (TS), the astropause (AP) and the bow shock (BS) are plotted with white lines. Distances along X and Z axes are normalized to R_0.

and dust number density n_d is normalized to that in the ISM ($n_{d,ISM}$) for each magnitude of a_d. I.e. dimensionless number density of all particles in the ISM is unity. We have omitted the sign "hat" to simplify notations. We consider only a part of the trajectory between the BS and the AP, which are located, respectively, at $z \approx 5$ and $z \approx 1$. Figs 4B and 4C plot the y- and z-components of the plasma ($\mathbf{v}_p$) and dust ($\mathbf{v}_d$) velocities. The x-components of these velocities are close to zero and we do not shown them. It is seen that the dust particle rotates in the (ZY)-plane and is moving together with the plasma (i.e. the dust velocity oscillates around the plasma velocity). $|v_{p,z}|$ decreases and $v_{p,y}$ increases with approaching to the AP, which is caused by the plasma deceleration and flowing around the AP.

Figs 5 and 6 plot the dust number density (n_d) and projection of the averaged dust velocity vector ($\mathbf{V}_{d,av}$) in

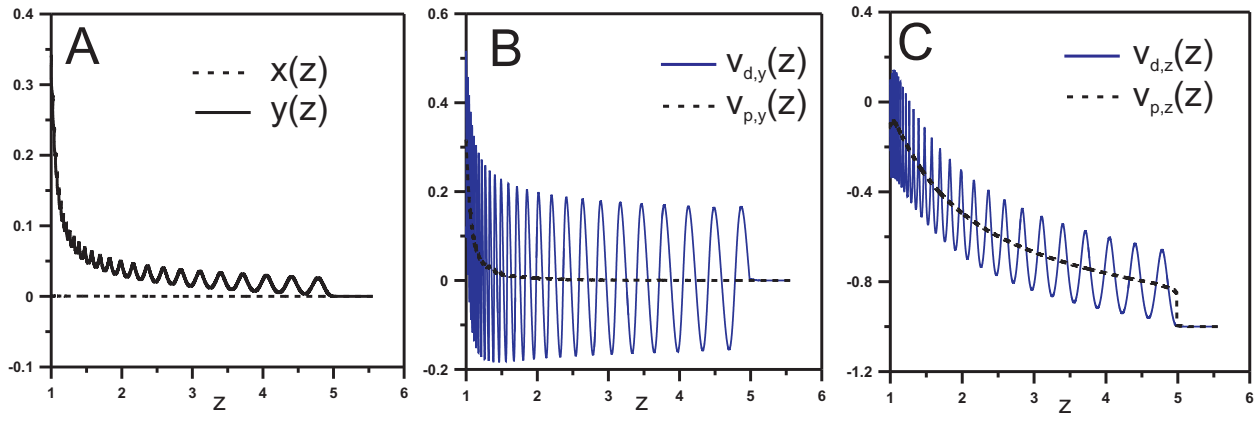

Figure 4. Example of one trajectory of a dust grain with $a_d = 5.4$. The trajectory is started at P_0. Plot A shows $x(z)$ and $y(z)$, plots B and C show y- and z-velocity components of the plasma and dust along the trajectory. All distances are normalized to R_0, velocities are normalized to V_{ISM}.

the (ZX)-plane. One can see that the dust distribution in the astrosphere is significantly non-uniform and non-monotonic. Several filamentary or cirrus-like structures (alternating maxima and minima of the dust number density) are clearly seen and their amount depends on a_d. The ratio of the maximum number density to the minimum one is about $2-4$.

To understand the origin of these non-monotonic behavior of the dust number density let us first consider the averaged velocity of dust grains with moderate value of a_d=1.8: the 2D plot of $|V_{d,av,z}|$ in the (ZX)-plane is shown in Fig. 7 A and the 1D plot in the upwind direction is shown in Fig. 7 B (together with the dust number density). From the 2D plot it is seen that the distribution of the dust averaged velocity also has the filamentary structure with several minima of the $|V_{d,av,z}|$-component. Positions of these velocity minima correspond to positions of maxima of the number density (it is clear from Fig. 7 B), i.e. dust accumulates in the regions of its deceleration. This is consistent with the continuity equation. Thus, dust number density is not uniform in the astrosphere due to periodical deceleration and acceleration of the dust grains. This non-monotonic behavior of the dust velocity is caused by gyrorotation around magnetic field lines. For example, for the trajectory started at point P_0 gyrorotation takes place in (Z,Y)-plane, and during each rotation at the point with maximal y, velocity vector of gyromotion is opposite to the plasma velocity and, hence, the total individual dust velocity has a minimum; oppositely, at the point with minimal y, total velocity has a maximum (see schematic illustration of this effect in Fig. 8).

The distance between the density maxima and their number depend on the period of gyrorotation of dust grains (see Fig. 8). Namely, in the case of the uniform electromagnetic field the distance between two adjacent maxima of $y(z)$ along the trajectory is equal to $D_{\rm gyr} = v_{p,z} T_{\rm gyr}$, where the dimensionless period of gyrorotation is $T_{\rm gyr} = 2\pi/(B a_{\rm d})$. In our case of changing $v_{p,z}$ and B along the trajectory distance between the density maxima depends on the averaged $D_{\rm gyr}$ at each part of the trajectory (values of $D_{\rm gyr}$ averaged over the whole trajectory are given in Table 2).

Fig. 9A shows $y(z)$ along the trajectories (started at P_0) for different a_d. It is seen that the grains are involved in the gyrorotation with corresponding gyroradius (given in Table 2). Distance between adjacent maxima of $y(z)$ along the trajectory correspond to the distance between maxima of the dust number density in Figs 5 and 6. Fig. 9 B shows D_{gyr} as a function of z for the trajectories started at P_0 and the all considered values of $a_{\rm d}$. Note that $D_{\rm gyr}$ decreases with approaching to the AP because the magnetic field B increases (see Fig. 3B). This is why the dust density filaments become more frequent close to the AP (see Fig. 5).

Note that the dust grains with $a_{\rm d} > 0.09$ almost do not penetrate through the AP because of relatively small gyroradius. The dust grains follow the magnetic field lines frozen in the plasma and cannot cross the AP. Particles of fairly large size ($a_{\rm d} = 0.09$, let us remind that a_d is inversely proportional to square of grain's radius) have the dimensionless gyroradius of $\sim$1.6, which this is enough to penetration inside the AP (see Fig. 6 D).

It is also interesting to examine Fig. 6C (for $a_{\rm d} = 0.18$). It is seen that there is one pronounced maximum of the dust number density and this maximum do not touch the AP. Therefore, the following situation is possible. Let us imagine that we observe an astrosphere due to emission of the interstellar dust and see one filamentary structure corresponding to the maximum of the dust number density. It is possible that the position of this observed filament does not coincide with the AP and the BS. So, it is important for the data analysis that usually we cannot observe the AP and the BS directly, but only what we see is the dust distribution in the astrosphere, which can be quite complicated. Detailed numerical MHD modelling of dust distribution in astrospheres is, therefore, needed for correct interpretation of observations.

3.2.2 Parallel case

Here we consider the parallel case, which is simpler than the perpendicular one because the magnetic field vector is always parallel to the plasma velocity vector (see, e.g., Baranov & Zaitsev 1995). Therefore, $E = -\mathbf{v}_p \times \mathbf{B} = 0$ and motion of the dust grains is a sum of gyrorotation around magnetic field lines, motion along field lines (with constant

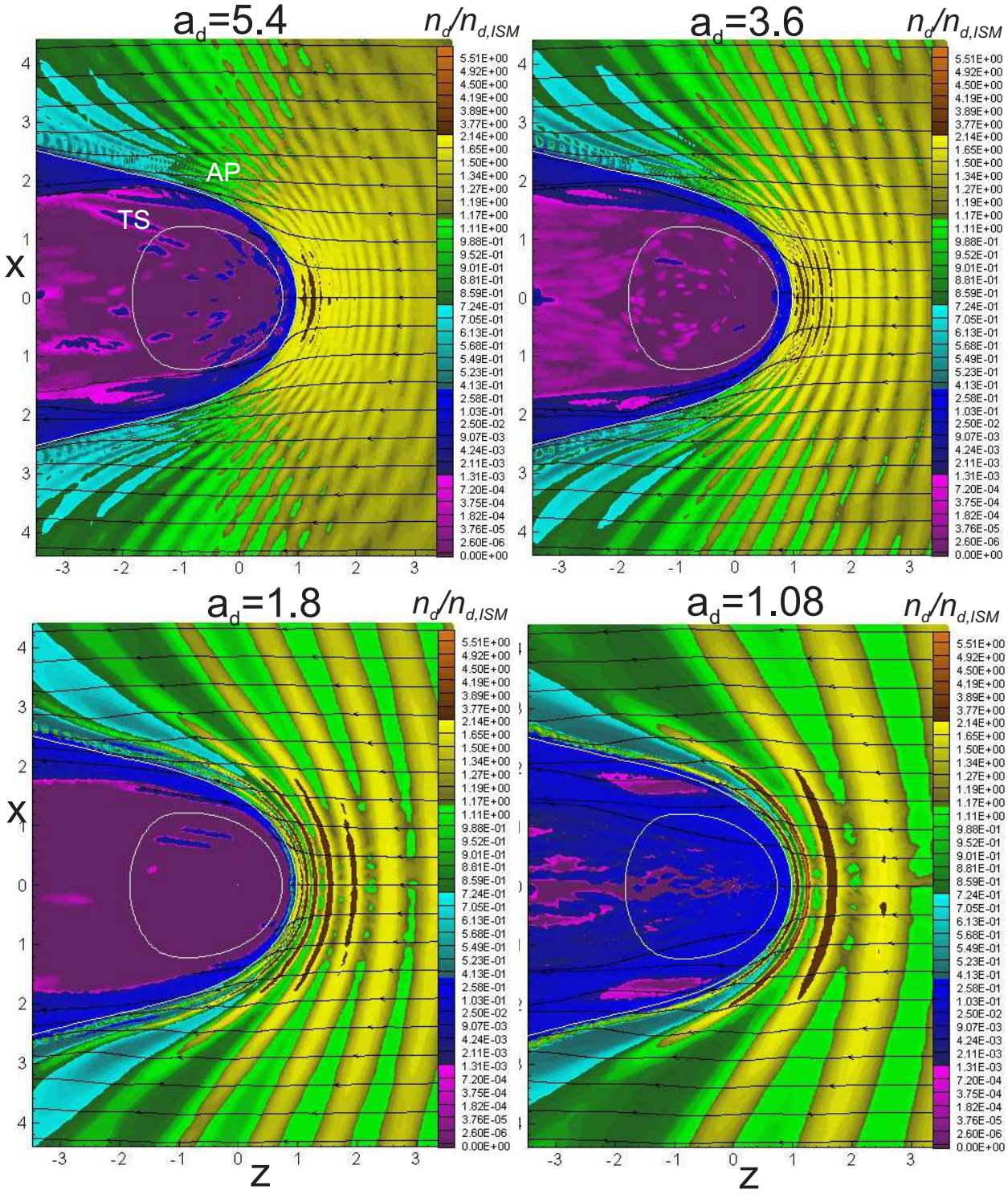

Figure 5. 2D distributions of the dust number density and streamlines in the (Z, X)-plane for the dust grains with different a_d obtained for the perpendicular case. The termination shock (TS) and the astropause (AP) are shown in all plots by white lines. Distances are normalized to R_0.

velocity $v_{\parallel} = \mathbf{V}_{\rm ISM}$) and drifts due to spatial gradients of the magnetic field.

Fig. 10 shows the interstellar dust number density and streamlines in the (ZX)-plane for a_d =7.2, 3.6, 1.8, 0.9. The periodical filamentary structures are clearly seen in the distributions. The physical mechanism of formation of such structures is the same as discussed in the previous section and is caused by the gyrorotation of the dust grains. It is interesting that in the parallel case all dust grains can penetrate through the nose region of the AP (i.e. the region around the critical point) where the plasma velocity and the magnetic field are zero.

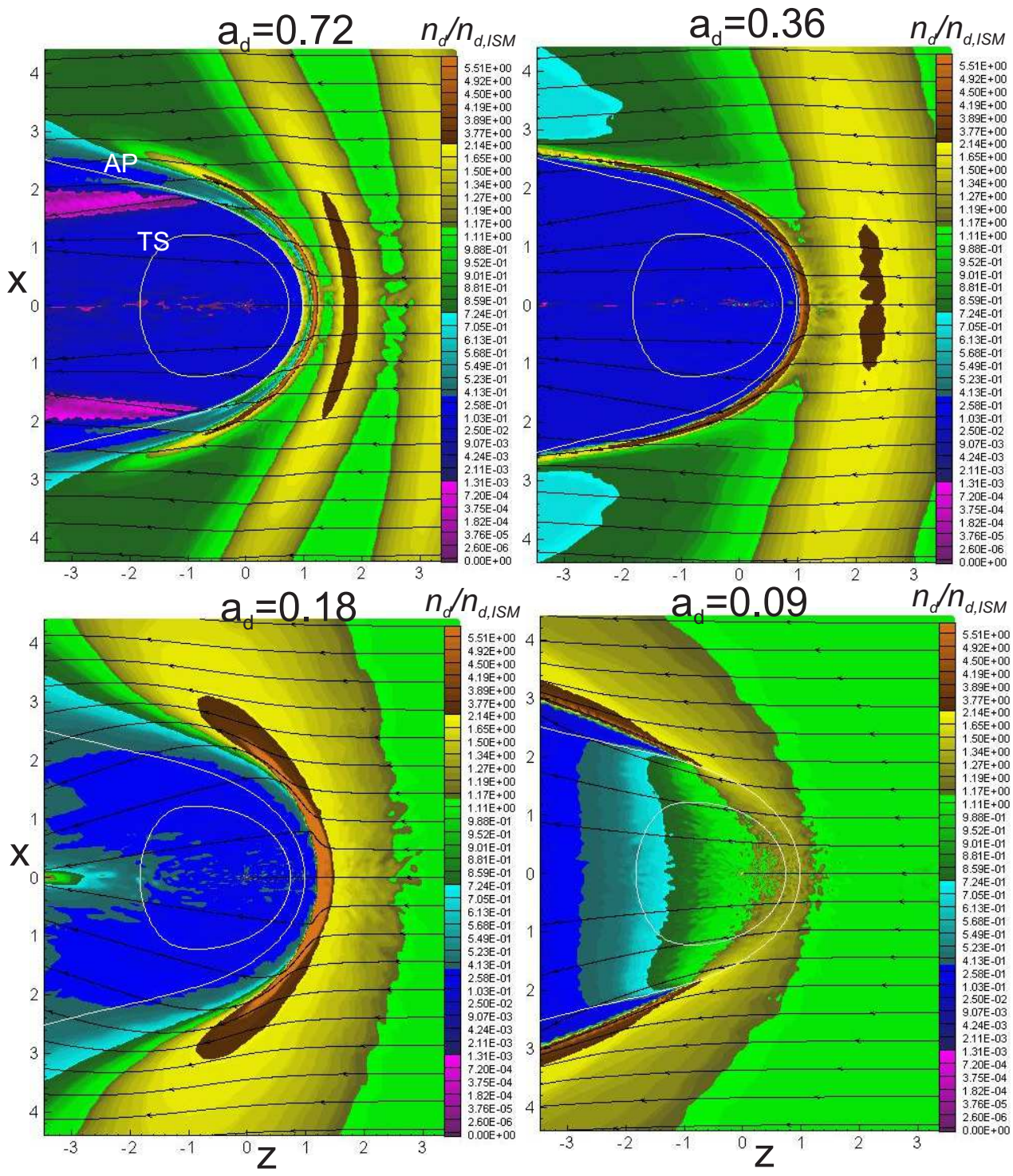

Figure 6. 2D distributions of the dust number density and streamlines in the (Z, X)-plane for the dust grains with different a_d obtained for the perpendicular case. The termination shock (TS) and the astropause (AP) are shown in all plots by white lines. Distances are normalized to R_0.

The presented results show that the filamentary dust distribution in astrospheres can arise both in the perpendicular and parallel cases. In the more general case of oblique magnetic field the overall qualitative picture remains the same, but the emerging filamentary structure is more complicated due to asymmetric MHD-structure of the astrosphere.

3.3 Shapes of astrosphere for different lines-of-sight

The filamentary, cirrus-like structure of astrospheres was revealed with modern infrared telescopes (see Section 1). Since the infrared emission of astrospheres around hot stars is mostly due to the absorption of stellar ultraviolet emission

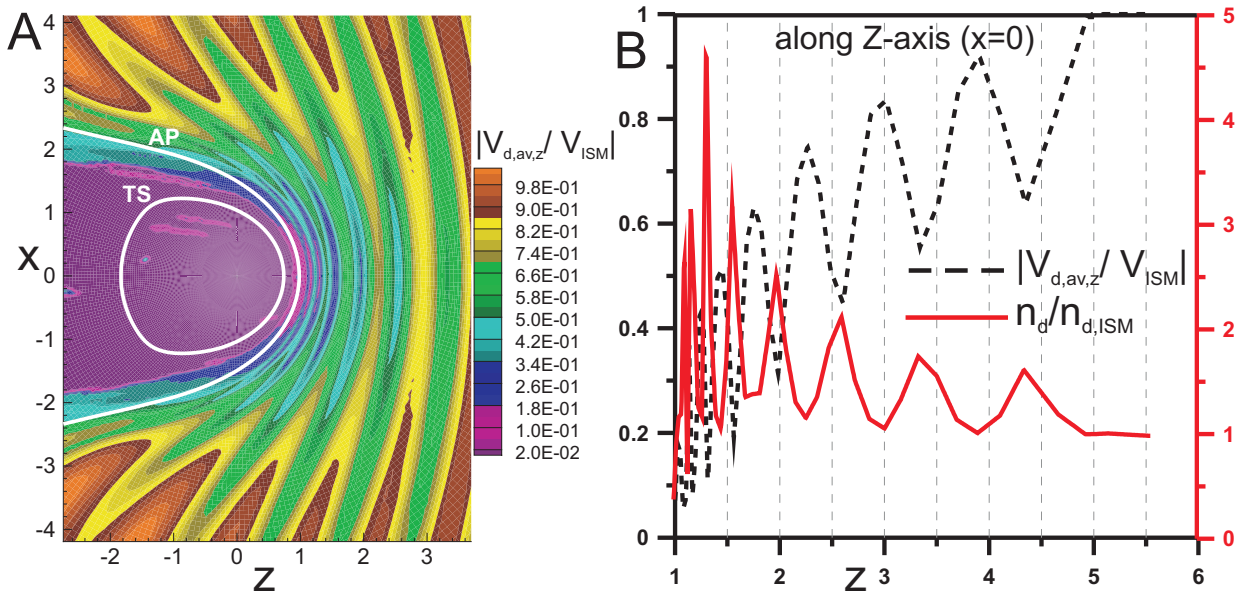

Figure 7. A. 2D distribution of the averaged dust z-velocity component (absolute value) in the (ZX)-plane obtained for the perpendicular case. B. Dust number density and averaged velocity (absolute value of the z-component) along the Z-axis (x=0, y=0). All results are presented for the dust grains with a_d=1.8. Distances are normalized to R_0.

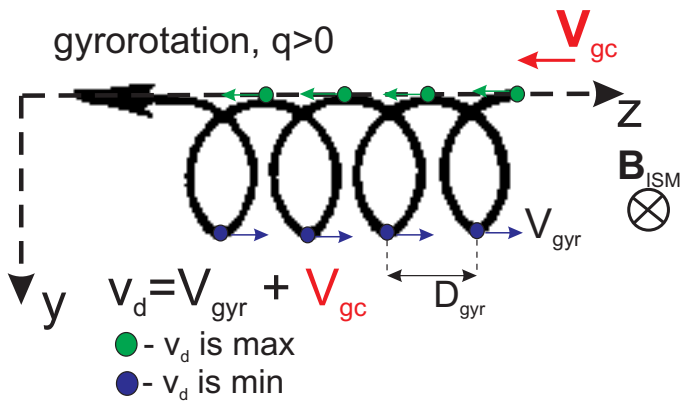

Figure 8. Schematic picture of dust grain motion in the uniform perpendicular magnetic field. Green dots correspond to maxima of the local dust velocity, blue dots correspond to the local minima (see text for details).

and its re-emission at longer wavelengths (e.g. van Buren & McCray 1988), it is naturally to attribute the observed filamentary structures to the specific dust distribution in astrospheres. The spectral characteristics of the resulting infrared emission are determined by the dust grain's properties and temperature, which, generally speaking, depends on the distance from the central star. However, in this work we do not consider the radiative transfer and its effect on the dust grains, which do not allow us to determine the dust temperature and precludes us from quantitative comparison of our model astrospheres with the observed ones. To make things simpler, we assume that the dust temperature is constant and does not depend on grain's size, so that the observed intensity of the infrared emission is proportional to the column number density of the dust particles, i.e. the integral of the dust number density along our line-of-sight.

In previous sections we presented the spatial distribution of the dust number density in the (ZX)-plane. Now we will consider how our model astrospheres will appear for different lines of sight, defined by angles θ and ϕ as specified in Fig. 11.

For the sake of illustration, we choose four lines of sight in the (ZY)-plane (i.e. ϕ=90°), with $\theta = 90°$, 60°, 45° and 30°. Fig. 12 plots 2D maps of integrated dust number density along the chosen lines of sight. Calculations are performed for the perpendicular case and the dust grains with a_d=1.8. One can see that the number of observed filaments depends on the orientation of the line of sight, i.e. for the larger θ one can distinguish the larger number of filaments at the nose part of the astrosphere. This is caused by simple geometrical effect: when we observe an astrosphere with acute θ different filaments overlap each other and are seen as one filament in the plane perpendicular to the line-of-sight.

Note that enhancement of the intensity seen in the tail part of the astrosphere is caused by the 3D features of the dust distribution. Namely, the dust flows around the as-

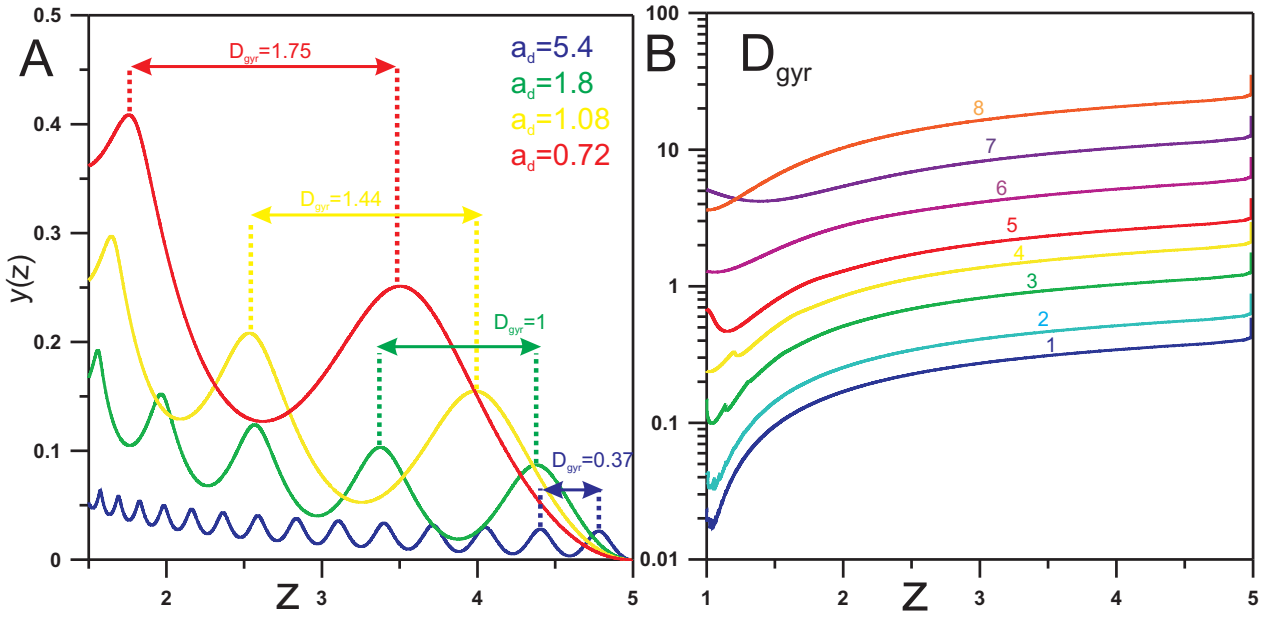

Figure 9. A. The trajectory ($y(z)$) started at P_0 is shown for dust grains with four different a_d. Periodical maxima and minima of $y(z)$ show the gyromotion of the dust grains with different gyroradii. The distance between adjacent maxima is marked by D_{gyr}. B. Results of calculations of $D_{gyr} = v_{p,z} \cdot T_{gyr}$ along the trajectory are shown for all considered dust grains. All distances (z, y, D_{gyr}) are normalized to R_0.

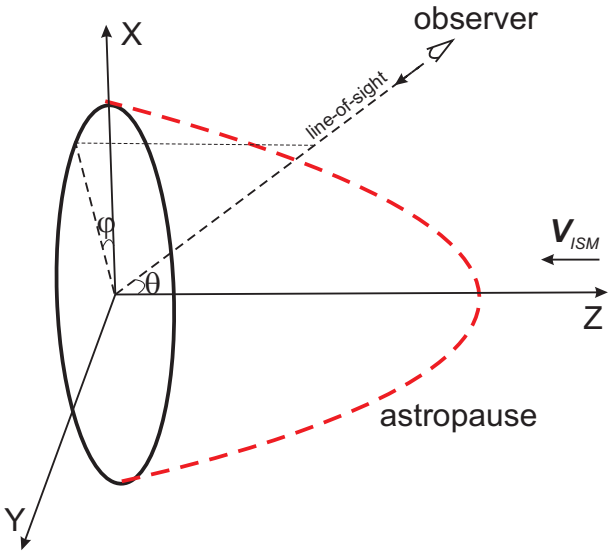

Figure 11. Schematic representation of observation of an astrosphere from an arbitrary line of sight. The astropause is shown by red dashed line. Line-of-sight is characterized by two spherical angles: θ and ϕ.

tropause, accumulates at flanks in (ZY)-plane and produce such maxima in the observational plane due to an integration of the number density along the line-of-sight.

The presented results show that the observed structure of astrosphere significantly depends on the angle between the line of sight and the direction of stellar motion. This means that for correct interpretation of observations the knowledge of both the 3D distribution of dust grains in the astrosphere and the velocity vector of the central star might be of crucial importance.

Table 3. Radii of dust grains (in μm) as a function of a_d for two sets of dimensional parameters of the astrosphere. Set 1: R_0=0.1 pc, $n_{\rm ISM}$=0.1 cm^{-3}. Set 2: R_0=1 pc, $n_{\rm ISM}$=1 cm^{-3}.

a_d	5.4	3.6	1.8	1.08	0.72	0.36	0.18
set 1	0.13	0.16	0.23	0.30	0.37	0.53	0.74
set 2	0.76	0.94	1.33	1.71	2.10	2.97	4.20

3.4 Transformation of a_d to the dust grain's radius

It is instructive to transform the dimensionless parameter $a_{\rm d}$ to the size of the dust grains in order to check whether such grains may exist in the ISM. From equations (1) and (5), one has:

$$a_d = \frac{q}{m}\frac{R_0\sqrt{\rho_{\rm ISM}}}{c_0} = \frac{q}{mc_0}\sqrt{\frac{\dot{M}v_{\rm w}}{4\pi V_{\rm ISM}^2}}. \qquad (6)$$

Thus, to obtain the dimensional value of q/m, one needs to specify either the stand-off distance of the astrosphere and the ISM plasma density, or the stellar wind mass loss rate and velocities of the stellar wind and the ISM flow. In principle, this could be done for each particular astrosphere. Here we consider typical ranges of observed stand-off distances $R_0 \sim 0.1-1$ pc and the ISM plasma number density $n_{\rm ISM} \sim 0.1-1$ cm^{-3}. The dust charge (in CGS units) can be expressed through the surface potential U and the radius of a dust grain $r_{\rm d}$, namely, $q = Ur_{\rm d}$. Assuming that the dust grains are spherical (with density $\rho_{\rm d}$ =2.5 g cm^{-3}), one has $q/m = 3U/(4\pi\rho_{\rm d}r_{\rm d}^2)$. As mentioned before, in this work we assume a constant dust grain charge (and surface potential) along the trajectory (this is discussed in the next section) and adopt the dust surface potential of U=+0.75 V, which is

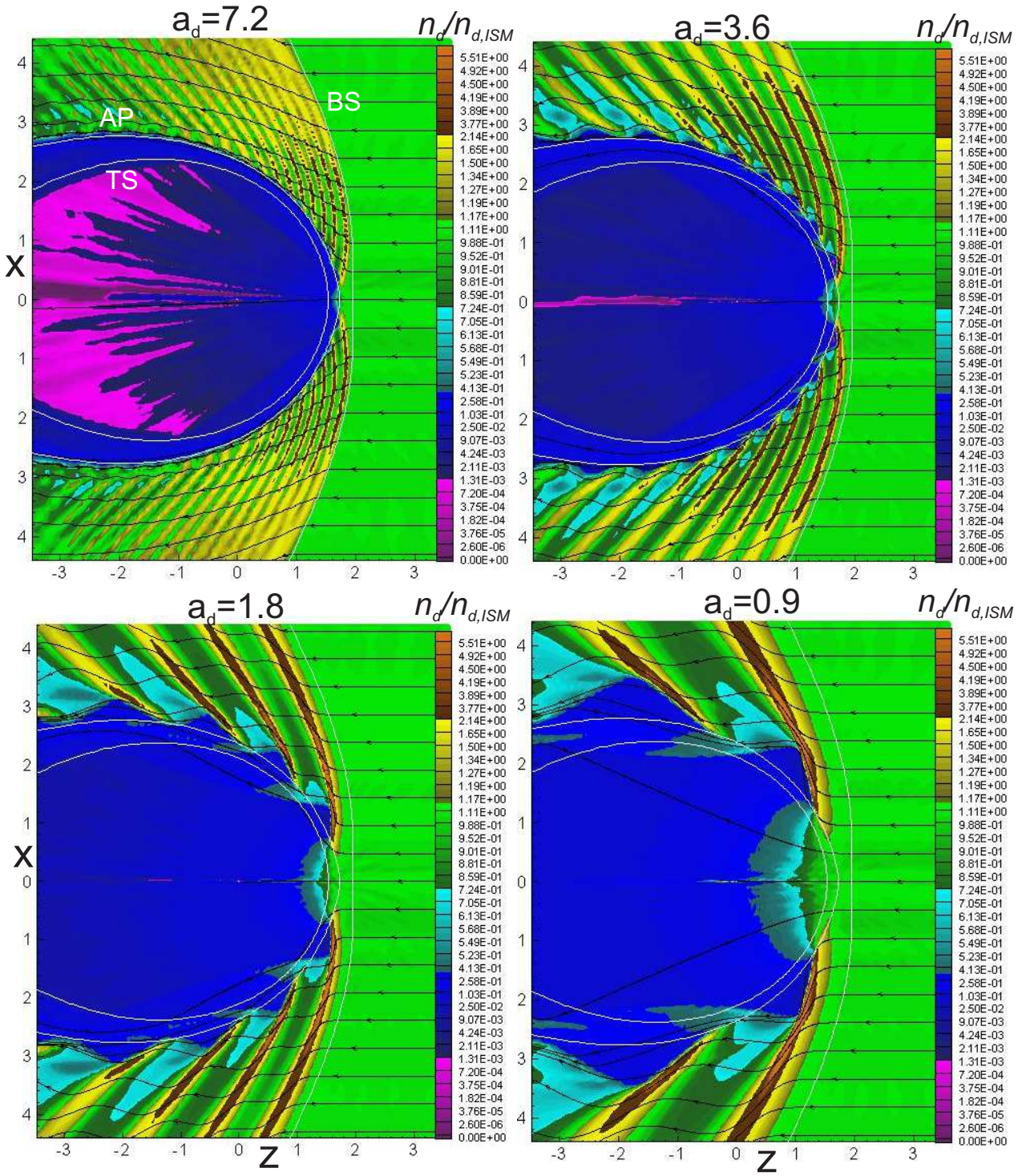

Figure 10. 2D distributions of the dust number density and streamlines in the (Z, X)-plane for the dust grains with different a_d obtained in the parallel case. The termination shock (TS), the astropause (AP) and the bow shock (BS) are shown in all plots by white lines. Distances are normalized to R_0.

typical for the dust in the Local interstellar medium around the Sun (Grün & Svestka 1996). The potential is usually positive due to an influence of accretion of protons, photoelectric emission of stellar and interstellar radiation and secondary electron emission (see, e.g. Kimura & Mann 1998; Akimkin et al. 2015).

Table 3 gives radii of dust grains for $a_d = 0.18 - 5.4$ and two sets of values of parameters R_0 and $n_{\rm ISM}$ (set 1: R_0=0.1 pc, $n_{\rm ISM}$=0.1 cm^{-3}; set 2: R_0=1 pc, $n_{\rm ISM}$=1 cm^{-3}). As it is seen from Figs 5 and 6, the filamentary structure exists for these magnitudes of a_d (for smaller and larger values of a_d the filaments either do not exist or non-visible). For set 1 we obtain the grains radii of 0.13-0.74 μm, and for set 2 the grains radii are 0.76-4.2 μm. In the classical MRN

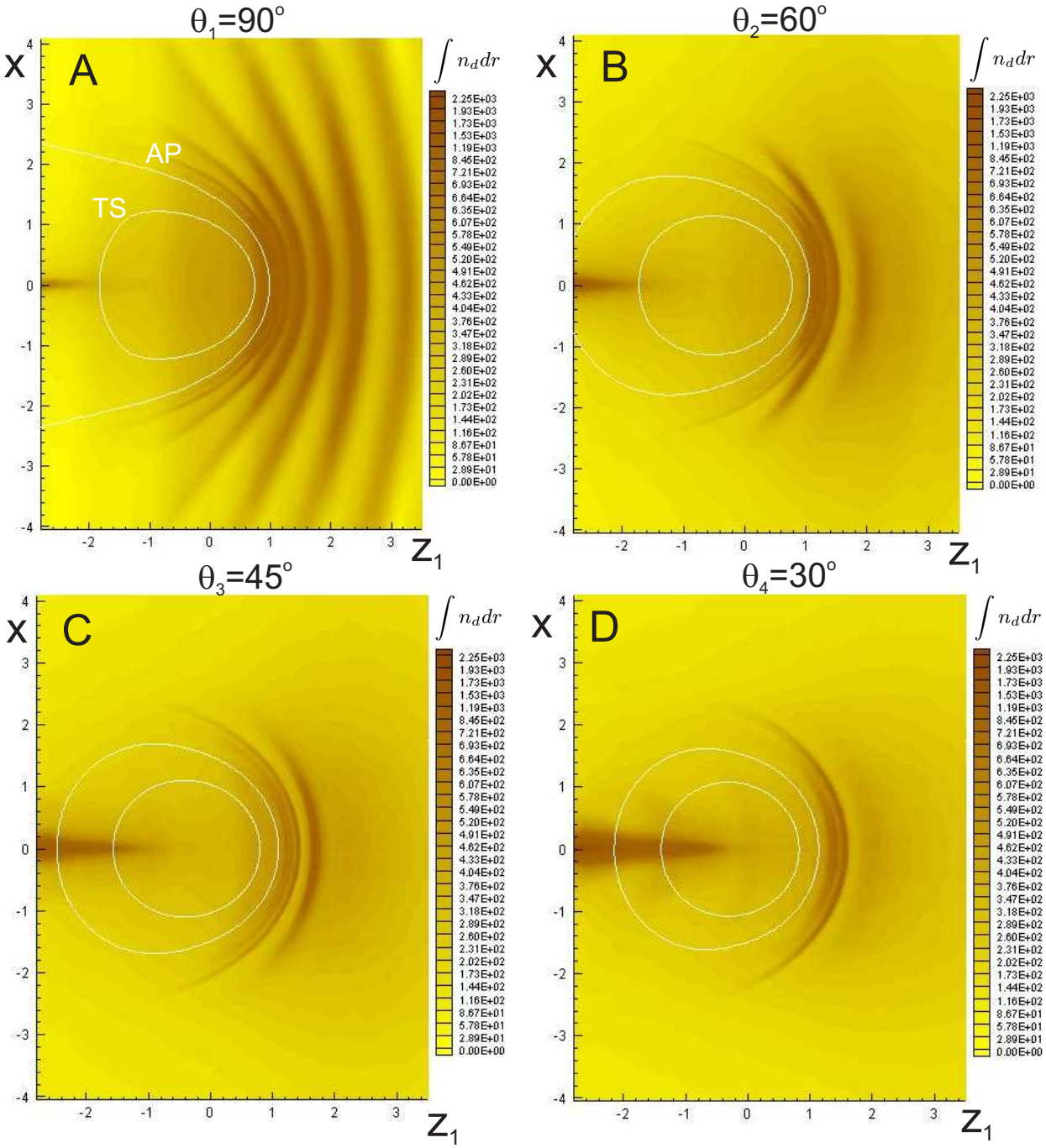

Figure 12. 2D maps of integrated dust number density along four lines of sight in the (ZY)-plane (ϕ=90°), with θ = 90°, 60°, 45° and 30°. Results are presented for the plane XZ_1 that is perpendicular to the line-of-sight. Projections of the termination shock (TS) and astropause (AP) on this plana are shown by white lines. The maps are obtained for the perpendicular case and the dust grains with $a_d = 1.8$. Distances are normalized to R_0.

(Mathis et al. 1977) size distribution of interstellar dust grains the radii of the grains range from 0.005 to 1 μm for graphite and from 0.025 to 0.25 μm for silicate. Therefore, the size ranges of the dust grains required for the filamentary structure in our model is within the MRN size-distribution for set 1 and has intersection with the MRN distribution for set 2. Also, Wang et al. (2015) stated that there are several independent observational evidences of presence of the very large dust grains in the ISM. They constrained the size distribution of the μm-sized dust population by fitting the observed mid-IR extinction at ∼3-8 μm in terms of the silicate-graphite-PAH model together with an extra population of μm-sized grains. They obtained the size-distribution of dust at the following ranges: 0.0001-0.4 μm for silicate and PAH, and two ranges 0.0001-0.4 μm and 0.5-6 μm for graphite. Therefore, the size ranges of the dust grains required in our model for formation of filamentary structures seems to be realistic especially in view of the facts that small

dust grains can be swept out from astrospheres (Ochsendorf et al. 2014) or destroyed (Pavlyuchenkov et al. 2013) by the stellar radiation.

4 DISCUSSION: LIMITATIONS OF THE MODEL

Now we discuss several limitations of our model, which we are going to improve in the future.

The first one is the neglecting of the drag force due to interaction of dust grains with protons and electrons through direct and Coulomb collisions (Draine & Salpeter 1979). Several authors take this force into account in simulations of the interstellar dust motion in astrospheres and H II regions (see, e.g., Ochsendorf et al. 2014; Akimkin et al. 2015). The drag force depends on the dust radius, relative velocity between plasma and dust (v_{rel}), plasma number density ($n_p = \rho/m_p$) and temperature (T). Namely, $F_{drag} = r_d^2\, n_p\, kT \cdot \hat{G}(v_{rel}, T)$, where k is the Boltzmann constant, $\hat{G}$ is dimensionless function, presented e.g. by Draine & Salpeter (1979). With this force the dimensionless motion equation (4) can be rewritten as:

$$\dot{\hat{\mathbf{v}}}_d = a_d[(\hat{\mathbf{v}}_d - \hat{\mathbf{v}}_p) \times \hat{\mathbf{B}}] + b_d \cdot \hat{p}\, \hat{G}(\hat{v}_{rel}, \hat{T}),$$

where dimensionless coefficient related to the drag force is the following:

$$b_d = \frac{R_0 \cdot \rho_{ISM} \cdot r_d^2}{m}.$$

Therefore, with substitution of equation (5) and expression for $q = U \cdot r_d$ one has:

$$\frac{b_d}{a_d} = \frac{R_0\, \rho_{ISM}\, r_d^2\, c_0}{U\, r_d\, \sqrt{\rho_{ISM}}\, R_0} = \frac{c_0}{U} \cdot \sqrt{\rho_{ISM}}\, r_d. \qquad (7)$$

Thus, an importance of the drag force relative to the Lorentz force is larger for bigger grain radii and plasma density.

We estimated acceleration of a dust grain (of a quite large radius of r_d=1 μm) due to the drag and Lorentz forces separately for the typical ISM parameters: $T_{\rm ISM} = 8\,000$ K, $n_{\rm ISM} = 0.1 - 1$ cm^{-3}, $V_{\rm ISM}$=25 km s^{-1} and R_0=1 pc. The results are shown in Fig. 13. It is seen that even for $n_{\rm ISM} = 1$ cm^{-3} the acceleration related with the drag force is almost two orders of magnitude smaller than the acceleration caused by the Lorentz force. Thus, the drag force can only be important either for very large grains (with radii of tens of microns) or for very dense ISM (with $n_{\rm ISM} \gtrsim 10$ cm^{-3}). Since none of these cases is considered in our simulations, we neglect the drag force.

The second limitation of our model is the assumption of constant dust grain charge along the trajectory. The charge of dust grains is controlled by three main processes: impinging of plasma particles (protons and electrons), secondary electron emission due to electron impacts (this process is important in regions of hot plasma with $T \gtrsim 10^5$ K) and photoelectron emission due to stellar and interstellar radiation. In principle, our model allows us to take changes of charge into account (we did this in the case of the heliosphere, see Alexashov et al. 2016). Our study of dust charge in the heliosphere shows that the largest changes occur in the solar wind region (i.e. inside the heliopause, which is an analogue of the astropause, see Fig. 2 in Alexashov et al., 2016). In this work we do not consider the dust dynamics inside the astropause. We estimate variations of the charge due to changes of the plasma density and temperature at the bow shock and in the interaction region between the BS and the AP, and find that they are not larger than 30 %. For simplicity, we neglect these changes and assume that the dust charge is constant. Note that in the case of massive hot stars the dust charge can be mostly influenced by the stellar radiation, which decreases with distance from the star as $1/r^2$. This may lead to changes of charge in the astrosphere if the layer between the BS and the AP is thick enough. Corresponding estimations of this effect should be done for each certain astrosphere. It should be noted also that possible variations of the charge will change the gyroradius of dust grains, which in turn will change the distance between the filaments.

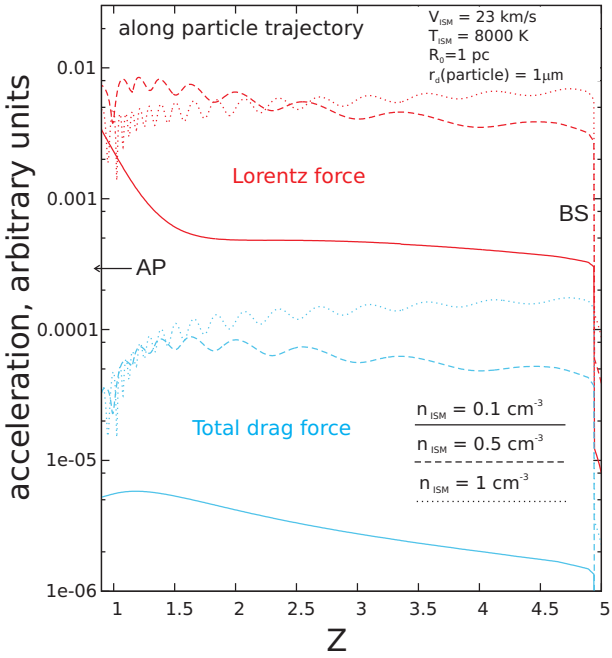

Figure 13. Acceleration of a dust grain due to Lorentz and drag forces along its trajectory. Radius of grain is 1 μm. Results are presented for three magnitudes of the ISM plasma number density (solid curves correspond to n_{ISM}=0.1 cm^{-3}, dashed curves correspond to n_{ISM}=0.5 cm^{-3}, and dotted curves correspond to n_{ISM}=1 cm^{-3}).

The third aspect that should be considered further is the realistic size distribution for the ISM dust grains. In this work we perform calculations for dust grains with a fixed size (characterized by the chosen parameter $a_{\rm d}$) separately, while in reality there are dust grains with a range of sizes (see, e.g., Mathis et al. 1977; Wang et al. 2015). The standard MRN size distribution is a $r_d^{-3.5}$ power law in grain radii, i.e. amount of the smallest grains is the largest. Thus, if we will calculate the dust column number density from particles of all sizes, then the contribution from the smallest grains will prevail and no filaments will appear (because the filaments produced by these grains are very narrow and the separation between them is too small). However, the effect of the small grains on the appearance of filaments would be negligible if they are swept out from astrospheres (Ochsendorf et al.

2014) or destroyed (Pavlyuchenkov et al. 2013) by the stellar radiation.

And the last limitation is that the observed intensity of the infrared emission from astrospheres depends not only on the dust column number density, but also on the dust temperature, which in its turn depends on the distance from the star and the physical parameters (size, composition) of the dust grains (see, e.g., Fig. 3 in Wang et al., 2015 and Eq. (14) in Decin et al., 2006). Hence, the relative contribution of the small and big dust grains to the total emissivity may be different and not simply proportional to their number densities. A radiative transfer model is needed for proper modelling of the dust heating and radiation (Pavlyuchenkov et al. 2013; Mackey et al. 2016). We are going to incorporate the radiative transfer code to our model in future works.

5 SUMMARY

In this work we investigate the spatial interstellar dust distribution in astrospheres with the interstellar magnetic field perpendicular and parallel to the velocity vector of the interstellar flow. We suggest a new physical mechanism for formation of filamentary structures observed for some astrospheres. It is shown that the alternating minima and maxima of the dust density occur between the astrospheric bow shock and the astropause due to periodical gyromotion of the dust grains. These filamentary structures appear in the model for particles with the period of gyration comparable to the characteristic time of the dust motion between the bow shock and the astropause.

More realistic numerical modelling and comparison with the observational data will be done in the future works.

ACKNOWLEDGMENTS

This work is supported by the Russian Science Foundation grant No. 14-12-01096.

REFERENCES

Akimkin V. V., Kirsanova M. S., Pavlyuchenkov Ya. N., Wiebe D. S., 2015, MNRAS, 449, 440
Alexashov D. B., Katushkina O. A., Izmodenov V. V., Akaev P. S., 2016, MNRAS, 458, 2553
Baranov V. B. & Zaitsev N. A., 1995, A&A, 304, 631
Baranov V. B., Krasnobaev K. V., Kulikovskii A. G., 1970, Dokl. Akad. Nauk SSSR, 194, 41
Comerón F., Kaper L., 1998, A&A, 338, 273
Cox N. L. G., et al., 2012, A&A, 537, A35
Decin L., Hony S., de Koter A., Tielens A. G. G. M., Waters L. B. F. M., 2012, A&A, 456, 549
Decin L., et al., 2012, A&A, 548, A113
Dgani R., Van Buren D., Noriega-Crespo A., 1996, ApJ, 461, 372
Draine B. T., Salpeter E. E., 1979, ApJ, 231, 77
Falle S. A. E. G., 1975, A&A, 43, 323
France K., McCandliss S. R., Lupu R. E., 2007, ApJ, 655, 920
Gvaramadze V. V., Bomans D. J., 2008, A&A, 490, 1071
Gvaramadze V. V., Langer N., Mackey J., 2012, MNRAS, 427, L50
Gvaramadze V. V., Kniazev A. Y., Kroupa P., Oh S., 2011a, A&A, 535, A29
Gvaramadze V. V., Röser S., Scholz R.-D., Schilbach E., 2011b, A&A, 529, A14
Grün E. & Svestka J., 1996, SSRev, 78, 347
Izmodenov V. V., Alexashov D. B., 2015, Astrophys. J. Suppl., 220, 32
Kimura H. & Mann I., 1998, ApJ, 499, 454
Kobulnicky H. A., Gilbert I. J., Kiminki D. C., 2010, ApJ, 710, 549
Kobulnicky H. A., et al., 2016, eprint arXiv:1609.02204
Mackey J., Haworth T. J., Gvaramadze V. V., Mohamed S., Langer N., Harries T. J., 2016, A&A, 596, A114
Mathis J. S., Rumpl W., Nordsieck K. H., 1977, ApJ, 217, 425
Meyer D. M.-A., Mackey J., Langer N., Gvaramadze V. V., Mignone A., Izzard R. G., Kaper, L., 2014, MNRAS, 444, 2754
Ochsendorf B. B., Cox N. L. J., Krijt S., Salgado F., Berné O., Bernard J. P., Kaper L., Tielens A. G. G. M., 2014, A&A, 563, A65
Pavlyuchenkov Y. N., Kirsanova M. S., Wiebe D. S., 2013, Astron. Rep., 57, 573
Peri C. S., Benaglia P., Brookes D. P., Stevens I. R., Isequilla N. L., 2012, A&A, 538, 108
Peri C. S., Benaglia P., Isequilla N. L., 2015, A&A, 578, 45
Sahai R., Chronopoulos C. K., 2010, ApJL, 711, L53
van Buren D., 1993, in Cassinelli J. P., Churchwell E. B., eds, ASP Conf. Ser. Vol. 35, Massive Stars: Their Lives in the Interstellar Medium. Astron. Soc. Pac., San Francisco, p. 315
van Buren D., McCray R., 1988, ApJ, 329, L93
van Buren D., Noriega-Crespo A., Dgani R., 1995, AJ, 110, 2914
Wang S., Aigen L., Jiang B. W., 2015, ApJ, 811, 38
Weaver R., McCray R., Castor J., Shapiro P., Moore R., 1977, ApJ, 218, 377
Wilkin F. P., 1996, ApJ, 459, L31